The X-ray absorption spectrum of O_2^+

Lucas M. Cornetta,[1] Ludvig Kjellsson,[2] Rafael C. Couto,[3] Hans Ågren,[2] Vincenzo Carravetta,[4] Stacey L. Sörensen,[5] Markus Kubin,[6] Christine Bülow,[6] Vicente Zamudio-Bayer,[6] Bernd von Issendorff,[7] J. Tobias Lau,[6,7] Johan Söderström,[2] Marcus Agåker,[2] Jan-Erik Rubensson,[2] and Rebecka Lindblad[5,6,8]

[1] *Instituto de Física, Universidade de São Paulo, Rua do Matão 1731, 05508-090 São Paulo, Brazil**
[2] *Department of Physics and Astronomy, Uppsala University*
[3] *Department of Chemistry, School of Engineering Sciences in Chemistry, Biotechnology and Health (CBH), KTH Royal Institute of Technology, SE-10044 Stockholm, Sweden*
[4] *IPCF-CNR, via Moruzzi 1, 56124 Pisa, Italy*
[5] *Department of Physics, Lund University, Sweden*
[6] *Abteilung für Hochempfindliche Röntgenspektroskopie, Helmholtz-Zentrum Berlin für Materialien und Energie, Germany*
[7] *Physikalisches Institut, Albert-Ludwigs-Universität Freiburg, Germany*
[8] *Inorganic Chemistry, Department of Chemistry - Ångström Laboratory, Uppsala University*

The X-ray absorption spectrum of the O_2^+ molecular cation has been measured. The ions were stored in a cryogenically cooled radiofrequency ion trap and probed by tunable synchrotron radiation. The spectrum exhibits several salient features - a three state composite π^*-resonance at the low energy side followed by a two-component exchange split, and highly dissociative, σ^*-resonance pulled down well below the ionization limit, and a complex valence-Rydberg high energy part, including several resolved bands. Small structures are interpreted as correlation state satellites with leading internal or semi-internal configurations. Calculations using the restricted active space wavefunctions and quantum wave packet dynamics offer an overall excellent interpretation of the spectral features.

I. INTRODUCTION

The capability to measure high-quality X-ray absorption spectra (XAS) of small molecular ions has generated a lot of new insights in recent years [1–13]. Apart from constituting a new challenge for fundamental molecular theory [14], the results are of relevance in many different fields: First, they provide reference data needed in ultrafast time-resolved experiments at high-harmonic generation and free-electron laser sources[15, 16]. Such data are especially important for attosecond transient absorption spectroscopy [17] where charge migration in molecular ions is investigated, but also for characterizing the background due to transient ionic species that are created in high-intensity experiments [18]. Second, the description of molecular ions are important for modelling plasmas of technical relevance, e.g. in the context of discharges and combustion [19]. Third, molecular ions are of astrophysical interest due to their role in planetary ionospheres [20] and interstellar clouds [21].

As a natural extension of earlier studies of cation near edge X-ray absorption fine structure (NEXAFS) addressing molecules with a closed shell in their neutral ground states, we here present and analyze the XAS spectrum of a molecule which is open shell in its neutral ground state - molecular oxygen, here measured at the ion trap end-station at the UE52-PGM beamline at the BESSY II synchrotron radiation facility [22, 23]. The spectrum was analyzed by means of the restricted active space computational technique for X-ray spectra [24] using implementations [25, 26] in the OpenMOLCAS program suite [27]. In this way it was possible to analyze the effects of relaxation and electron correlation with proper spin coupling. A wavepacket technique was used to characterize the vibrational fine structure.

Our work reveals several new phenomena with new insights. The $1s \rightarrow \pi^*$ excitation gives rise to three multiplets with vibrational progressions, similar to the corresponding excitation in the isoelectronic open-shell molecule NO [28]. While the same configuration is populated in core-level photoemission of the neutral molecule [29], the selection rules lead to population of states that have not been observed before. The second broad band is also novel in appearance - it is assigned to excitation to two dissociative $1s^{-1}\sigma^*$ states with different internal spin couplings, which, in contrast to the corresponding transitions in the XAS spectrum of neutral O_2, reside well below the ionization limits and are largely separated from Rydberg excitations. Closer to the ionization limits the spectrum exhibits a rich structure, which can be assigned to mixed valence-Rydberg and Rydberg transitions where states with internal and semi-internal excitation patterns can be assigned. The excellent agreement between observations and the predictions of RASPT2 theory demonstrates that the specific electron correlation effects associated with cationic XAS[6, 10, 11] are now fully taken into account.

* lucas.cornetta@usp.br

II. EXPERIMENTAL

The X-ray absorption spectrum of O_2^+ was measured using synchrotron radiation at the ion trap end-station at the UE52-PGM beamline at the BESSY II synchrotron radiation facility [22]. The same experimental procedure as in our earlier studies [6, 7, 10, 11] was used. Oxygen gas is leaked into a helium plasma, created by magnetron sputtering, where the molecules are excited and ionized. These ions are extracted from the source, O_2^+ ions are selected in a quadrupole mass filter and guided into a cryogenically cooled radiofrequency ion trap. Upon interaction with the synchrotron radiation the ions in the trap are excited and ionized, and the content of the trap is analyzed in a reflectron mass spectrometer. Mass spectra are recorded as the energy of the incident photon energy is varied. Here we assume that the yield of O^+ fragments is proportional to the X-ray absorption cross section of O_2^+.

The beamline energy was calibrated by a standard procedure using XAS of N_2 [30]. XAS of neutral O_2 was measured using a monochromator exit slit of 15 µm by electron yield in an upstream gas-cell and used for energy reference. The three regions of the O_2^+ spectrum, $528-565$ eV, $530.7-536$ eV, $541-558$ eV, were each recorded with a different monochromator exit slit. Overview with 100 µm, high energy with 50 µm, and the π^*-resonance with 15 µm, corresponding to estimated bandwidths of 130 meV, 70 meV and 20 meV.

III. THEORY

The simulations of the X-ray absorption spectrum were done by a combination of multiconfigurational electronic structure and nuclear wave packet dynamics methods, in similar fashion as in previous works [6, 7, 10, 11, 33]. State-average restricted active space self-consistent field (SA-RASSCF) calculations were performed [24–26], followed by multi-state second-order perturbation calculations (MS-RASPT2) [34]. Proper core-valence separation [35, 36] restrictions on the O1s core orbitals were imposed in order to avoid the variational collapse of the wave functions. Preliminary inspections of the XAS structure for O_2^+ suggest that in the 541-558 eV range features below the ionization threshold are characteristic of Rydberg states. Therefore, the ANO-RCC-VQZP basis set was used, together along an auxiliary Rydberg diffuse basis set for a proper description of such states (Table S1). For this auxiliary diffuse basis set a $8s8p8d8f \rightarrow [3s2p2d1f]$ contraction scheme has been used, in which the primitive functions were obtained from a preset Rydberg basis set proposed by Kaufmann [37]. Since we are dealing with Rydberg states supported by a cationic species, all the exponents in the basis set have been multiplied by a factor of four, ($\alpha \sim Z^2$...) before the contraction. Scalar relativistic effects are included by using a second-order Douglas-Kroll-Hess Hamiltonian [38, 39], in combination with the ANO-RCC basis. Transition dipole moments were obtained by the RAS state-interaction (RASSI) approach [40, 41]. Also, the orbitals were localized by the PIPEK-MEZEY procedure [42], and the calculations have been performed at the C_{2v} point group of symmetry. In the RASPT2 step, an imaginary shift of 0.3 Hartree [43] and the default ionization-potential electron-affinity (IPEA) shift of 0.25 Hartree [44] were applied. The potential energy curves have been computed considering the active space RAS(13,1,0;1,14,0) active space. The RASSCF active space is labeled RAS(n, l, m; i, j, k), where i, j, and k are the number of orbitals in RAS1, RAS2, and RAS3 spaces respectively, n is here the total number of electrons in the active space, l the maximum number of holes allowed in RAS1, and m the maximum number of electrons in RAS3. The state-average procedure was performed considering eight states for the π^* region and twelve states for the σ^* and high energy region.

The vibrationally-resolved spectrum was computed by means of quantum nuclear wave packet dynamics [45]. The absorption cross section as a function of the incident photon energy (ω) is resolved as the following sum over the excited states

$$\sigma(\omega) = \mathrm{Re}\sum_c \langle \nu_0 | \Psi_c(0) \rangle, \tag{1}$$

where

$$|\Psi_c(0)\rangle = D_{c0}\int_0^\infty e^{i(\omega-\omega_{c0}+\epsilon_{\nu_0}+i\Gamma_c)t}|\psi_c(t)\rangle dt. \tag{2}$$

In the above expression, D_{c0} depends on the transition dipole moment between the initial (ground) state and the excited state $\mathbf{d}_{c0}$ and the photon polarization vector $\mathbf{e}$ as in $D_{c0} = (\mathbf{e}\cdot\mathbf{d}_{c0})$, ω_{c0} is the vertical transition energy, ϵ_{ν_0} is the vibrational energy of the initial wave packet and Γ_c is the natural width associated with state c. The propagation of the wave packet on each excited state is given by

$$|\psi_c(t)\rangle = e^{-ih_c t}D_{c0}|\nu_0\rangle, \tag{3}$$

where h_c is the nuclear Hamiltonian related to electronic state c. All propagations were addressed within the split-operator technique in a spatial grid in of 2048 points. A total of 2^{18} timesteps was used for the time-evolution, with a total time of 10 fs. Equations 1 and 2 were solved with a half-Fourier transform with the use of the FFT algorithm. The initial wave packet $|\nu_0\rangle$ in all cases was set as the lowest vibrational level of the $^2\Pi$ ground state of O_2^+. The broadening of the vibrational profile is given by the lifetime broadening of the O_2 core-excited state taken from Coreno et al. [46], which corresponds to $\Gamma =$ 74.7 meV (HWHM). The spectrum related to each core-excited state was computed separately.

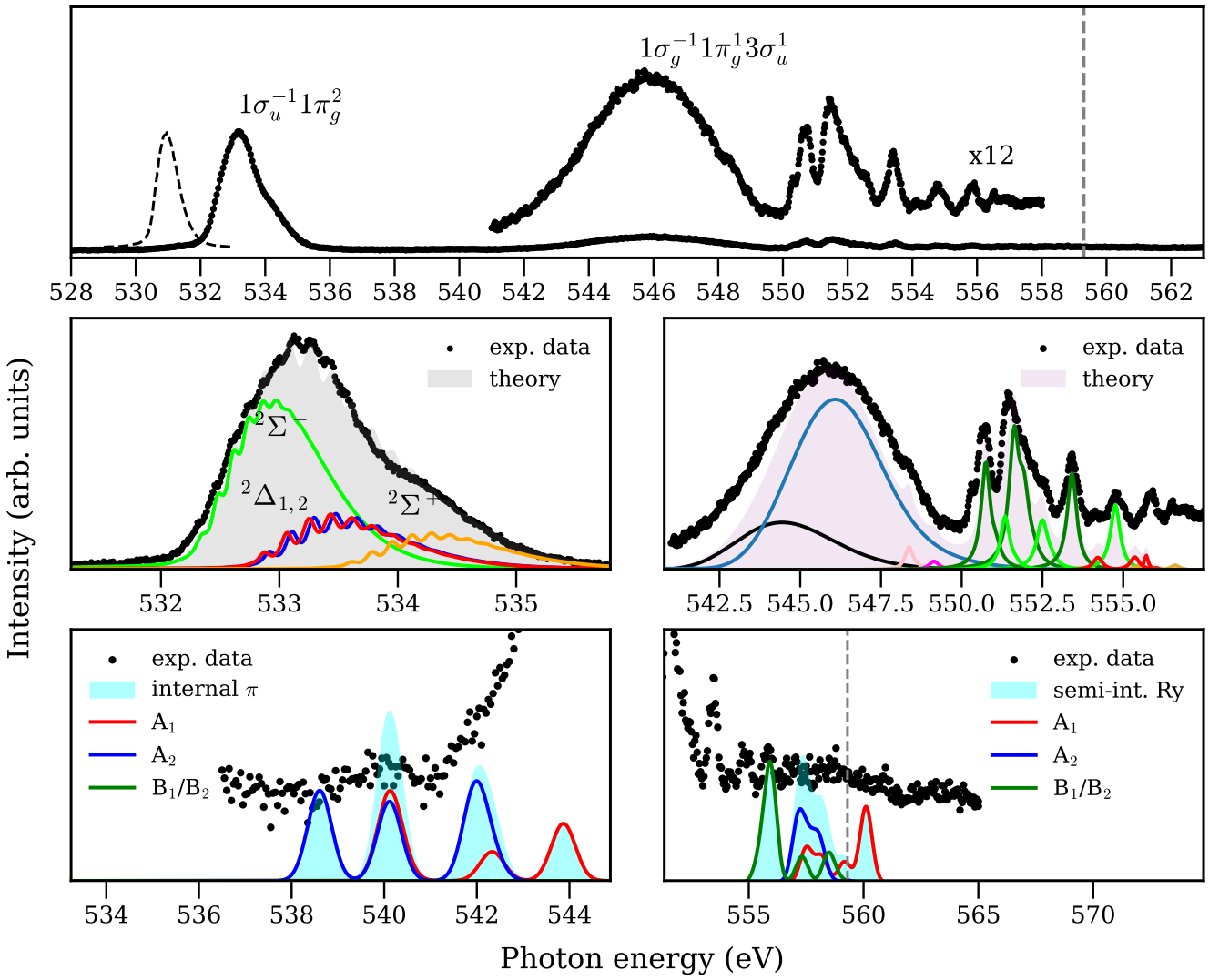

FIG. 1. (Top) The X-ray absorption spectrum of O_2^+. Neutral O_2 was measured at the O1s-π^* resonance for energy reference and is shown as a dashed line. The threshold for core ionization from the $^2\Pi_g$ ground state of the cation to the first $^3\Pi_{g,u}$ core-valence states of the dication, marked by a dashed vertical line, is estimated to be at 559.3 eV, by combining valence band [31] and core-valence [32] photoemission. (Middle) Theoretical absorption cross section for the π region (left) and the σ/high-energy region (right), together with the experimental data. The colors of each component of the spectrum respect the color schemes of the potential energy curves shown in Figures 3 and 4. (Bottom) Transitions related to $\pi_u\pi_g$ (left) and π_u/Ry (right) internal and semi-internal excitations (see text). The theoretical spectra have been shifted by -0.31 eV (π^* resonances, middle left), -1.2 eV (σ^* resonances, middle right) and +0.29 eV (Rydberg states - middle right - and semi-internal states - bottom).

IV. RESULTS AND DISCUSSION

The ground state of the molecular cation O_2^+ is a $^2\Pi_g$ multiplet state originating from the $1\sigma_g^2 1\sigma_u^2 2\sigma_g^2 2\sigma_u^2 3\sigma_g^2 1\pi_u^4 1\pi_g^1$ electronic configuration (Fig. S1). As in earlier XAS investigations of cationic small molecules we find it natural to separately discuss the spectra in the three regions in order of increasing energy: a "repopulation" band associated with filling the vacancy in the outermost orbital of the ion, a composite band of valence excitations, and a series of transitions featuring Rydberg – valence mixing with strong electron correlation. The XAS (Fig. 1) spectrum is dominated by a peak that reaches its maximum at 533.2 eV, and can be assigned to transitions to $1\sigma_u^{-1}1\pi_g^{+2}$ states, i.e., the outermost vacancy is filled. O_2^+ is isoelectronic with NO [28, 47, 48], and we expect qualitatively similar electronic coupling.

The broader feature appearing at 546 eV is the composite valence band, assigned to $1\sigma_g \rightarrow 3\sigma_u$ excitations. As in earlier studies of cationic XAS, the final state in this region has three open shells, the leading configura-

tion being $1\sigma_g 1\pi_g 3\sigma_u$ with the term $^2\Pi_u$. The internal spin coupling splits this state, and the lack of fine structure indicates that states are dissociative. The sharp peaks in the $550-558$ eV energy range are due to excitations of Rydberg and Rydberg-valence mixed character, and they also involve configurations with double excitations. In addition, we observe weak structures, that our analysis assigns to internal and semi-internal double excitations, involving the singly occupied $1\pi_g$ orbital. These transitions populate states where $1\sigma_g^{-1}1\pi_u^{-1}1\pi_g^{+2}$ and $1\sigma_g^{-1}1\pi_u^{-1}1\pi_g^{+1}nl^{+1}$ are leading configurations, nl denoting a Rydberg orbital. Such processes become feasible in ionic species with open shells.

Below we discuss these three energy regions in some detail.

A. The π^* resonance

The $1\sigma_u \rightarrow 1\pi_g$ peak exhibits vibrational fine structure (Fig. 1 middle left and Fig. 2 bottom) and contributions from several electronic states. In LS coupling, the final-state configuration $1\sigma_g^2 1\sigma_u^1 2\sigma_g^2 2\sigma_u^2 3\sigma_g^2 1\pi_u^4 1\pi_g^2$ gives the dipole allowed terms $^2\Sigma_u^-$, $^2\Delta_u$ and $^2\Sigma_u^+$ (Fig. 3).

It is instructive to compare to X-ray photoemission spectroscopy (XPS) of neutral O_2, as the same electronic configuration is reached in both cases. Here the allowed states are $^4\Sigma_{g/u}^-$ and $^2\Sigma_{g/u}^-$. In the middle panel of Fig 2 the ionization energy of neutral O_2 to the ground state of the ion, measured to be 12.074 eV[31] has been subtracted from the binding energy scale of the XPS spectrum [29] for comparison. It is clear that only the $^2\Sigma_u^-$ state is expected to be populated in both spectroscopies. It is immediately obvious that only doublet final states are observed in XAS of the ion, and that vibrational excitations are more prominent than in XPS. Sörensen *et al.* measured the energy and vibrational constants of the $^2\Sigma_{g/u}^-$-state from the XPS spectra, and theoretically they estimated the gerade-ungerade splitting to be ~ 7 meV [29]. The more extensive vibrational excitations in the NEXAFS case can be understood from the antibonding character of the $1\pi_g$ orbital, the population of which gives an additional bond extension compared to the opening of the bare oxygen core orbital[49].

In oxygen K edge XAS of the NO the $^2\Sigma_u^-$, $^2\Delta_u$, and $^2\Sigma_u^+$ final states give rise to a structured peak including vibrational excitations (Fig. 2 top), which has been thoroughly analyzed [28, 48] . The comparison between the spectra of NO and O_2^+ is motivated by their similar electronic configuration, term-designation, and mass. Indeed, the $1\sigma_u \rightarrow 1\pi_g$ resonance in O_2^+ and NO (Fig. 2) has a similar shape, with a threefold structure, although the O_2^+ peak appears at higher energy, is narrower than its NO counterpart, and the vibrational fine structure is not as clearly resolved.

The theoretical prediction (Fig. 1 middle left and Fig. 2 bottom) is in excellent agreement with the observed

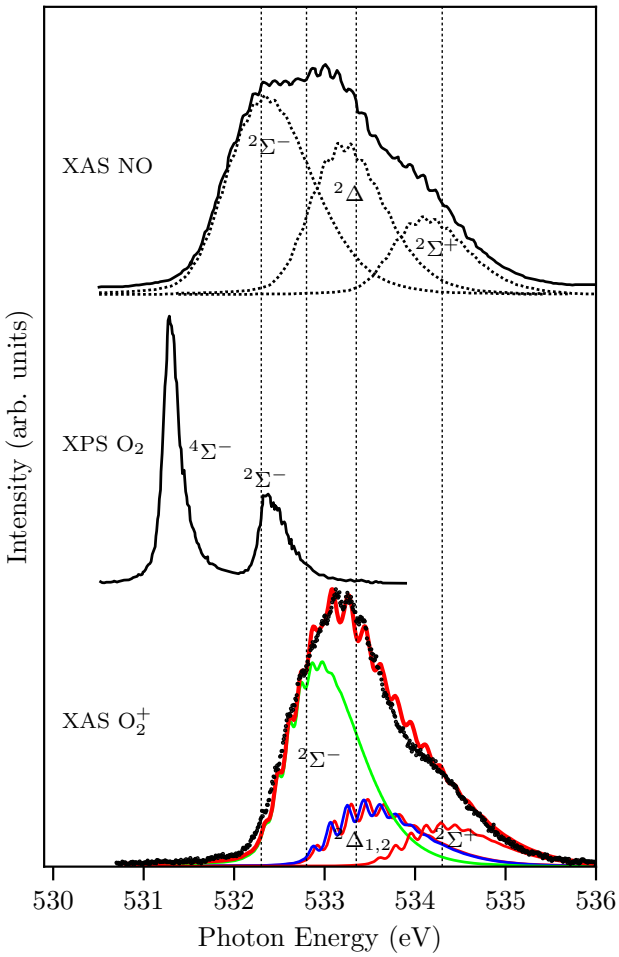

FIG. 2. A comparison between the O_2^+ XAS spectrum at the $1\sigma_u \rightarrow 1\pi_g$ resonance (bottom), the XPS spectrum of O_2 [29] (middle) and the O K edge XAS spectrum of NO [28] (top). For comparison, the XPS spectrum is shifted by subtracting the valence ionization energy [31] from the measured binding energy scale.

peak shape. It confirms that the ordering of the $^2\Sigma_u^-$, $^2\Delta_u$, and $^2\Sigma_u^+$ final states are the same as in the NO counterpart, and it gives two close-lying spin-orbit components of the $^2\Delta_u$ term. We see a large number of vibrational excitations in both the NO and O_2^+ spectra, and the similarities suggest that the $1\sigma_u \rightarrow 1\pi_g$ excitation leads to a similar bond elongation in the two cases. In Table I we list the theoretical constants for the observed states. Although it is difficult to extract the corresponding experimental values from the spectra, the overall agreement (Fig. 2) corroborates the theoretical values.

Finally, we compare the energy split due to π^2 coupling in three cases. Close to the $^3\Sigma_g^-$ ground state of neutral O_2, we find the two excited singlet-oxygen states, $^1\Delta_g$ and $^1\Sigma_g^+$. In the core excited doublet states of O_2^+, the three states directly correspond to the $^2\Sigma_u^-$, $^2\Delta_u$ and $^2\Sigma_u^+$

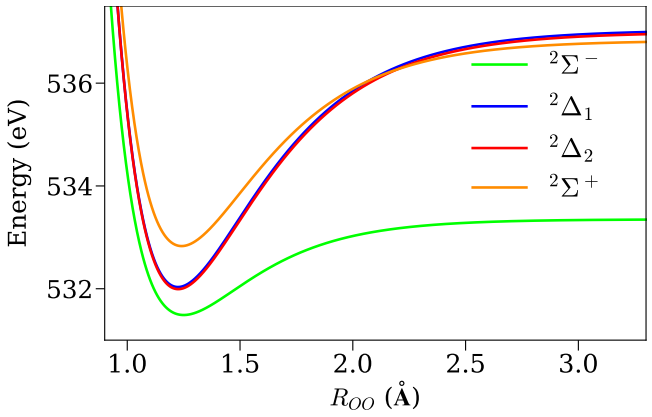

FIG. 3. Potential energy curves, in eV, for the first four core-excited states of O_2^+.

TABLE I. Theoretical molecular constants for O_2^+. E_{00} stands for the potencial energy minimum in relation to the ground state minimum, R_e is the equilibrium bond length, ω_e denotes the harmonic frequency and $\omega_e\chi_e$ is the anharmonicity constant.

State	E_{00} [eV]	R_e [Å]	ω_e [meV]	$\omega_e\chi_e$ [meV]
Ground state	-	1.118	234.5	2.1
$^2\Sigma^-$	531.49	1.250	140.2	2.6
$^2\Delta$	531.99	1.226	192.1	1.8
$^2\Delta$	532.03	1.225	192.5	1.9
$^2\Sigma^+$	532.83	1.241	176.4	1.9

states, where the only difference is due to the core hole. We note that the $^3\Sigma_g^-$ - $^1\Delta_g$ and the $^3\Sigma_g^-$ - $^1\Sigma_g^+$ separations close to the O_2 ground state are 1.0 eV, and 1.64 eV, respectively[50], while the corresponding values for core-excited O_2^+ are calculated to be 0.7 eV, and 1.6 eV. The similarity suggests that the extra unpaired core-electron contributes very little to the valence coupling, and that relaxation due to the core hole is of less importance. In line with the comparison in Fig. 2, the separation between the states in NO is somewhat larger, 1.1 eV and 2.0 eV for the $^3\Sigma_g^-$ - $^1\Delta_g$ and $^3\Sigma_g^-$ - $^1\Sigma_g^+$ separations, respectively[28].

B. The σ^* resonance

We assign the broad feature at around 546 eV (Fig. 1) to the $1\sigma_g \rightarrow 3\sigma_u$ resonance, and thus to the $^2\Pi_u$ final state of the $1\sigma_g^1 1\sigma_u^2 2\sigma_g^2 2\sigma_u^2 3\sigma_g^2 1\pi_u^4 1\pi_g^1 3\sigma_u^1$ configuration. For small molecules, this so-called σ^* resonance is generally situated in the continuum, often forming a shape resonance, or lying close to the ionization limit. In neutral O_2, the valence excited state interacts and overlaps with Rydberg states creating a complex spectral structure [51–53]. In the case of O_2^+ the σ^*-resonance is pulled deeply below the ionization limit, and is well separated from the Rydberg excitations. This is attributed to the stronger positive potential for the σ^* state in the ion. The width of the peak and its lack of fine structure is inline with the expectation that the state is dissociative. We show below that the unresolved structure comprises two states with two different internal spin-coupling involving the open shells, like in the neutral counterpart [51, 52] and in the XAS of other diatomic ions[6, 7]. The appearance of the σ^* resonance can also be qualified in light of earlier analysis of cationic NEXAFS spectra involving valence levels where these transitions are quite well described in an "extended one-electron picture" or a picture referring to the smallest possible linear combination of determinants that fulfill spatial and spin symmetry[10, 11]. Exchange interaction between the open shell orbitals serves as the main source for the energy splitting, where this interaction between valence HOMO and LUMO shells is generally stronger than that between core and any of these shells. The spatial distribution of the HOMO and LUMO orbitals is found to strongly dictate both the energy splitting and relative intensities. The potential curves for the two spin-coupled states are in general quite different, resulting in widely different vibrational progressions[10, 11]. Inspecting the computational results for O_2^+ we see similar features for the spin-coupled valence transitions, although in this case we have an open-shell ground state and valence level of σ^* character (instead of π^*), which moreover is strongly dissociative compared to the π^* states in N_2 and CO. Based on the excellent agreement with the predicted σ^* band shape, we can conclude that the splitting between the vertical energies for the two spin-components is about 2.5 eV and where the intensity of the upper component is dominant. The subtle dependence on exchange interaction dictates the final outcome, something that is well reproduced by the RAS calculations.

C. High energy correlation state transitions

Earlier recordings of the "third part" of cationic XAS spectra have shown wide, very irregular, but sharp, features. In contrast to neutral molecular XAS there is no or little indication of Rydberg series or mixed valence-Rydberg transitions. N_2^+ and CO^+ are perhaps the best examples exhibiting well defined spectroscopic features in this high energy part[6, 7]. There are a couple of reasons for this - one is that many of the correlated, two-electron two-hole transitions that appear above the ionization threshold in neutral molecules[54] are pulled down below the IP by the stronger potential of the cation where they mix with the Rydberg states. A number of such transitions with multiconfigurational character were assigned by MS-RASPT2 calculations in the previous works on N_2^+ and CO^+[6, 7].

A second reason for the appearance of distinct multi-electron states in the upper part of the spectra is that with an open valence shell in the initial state so-called

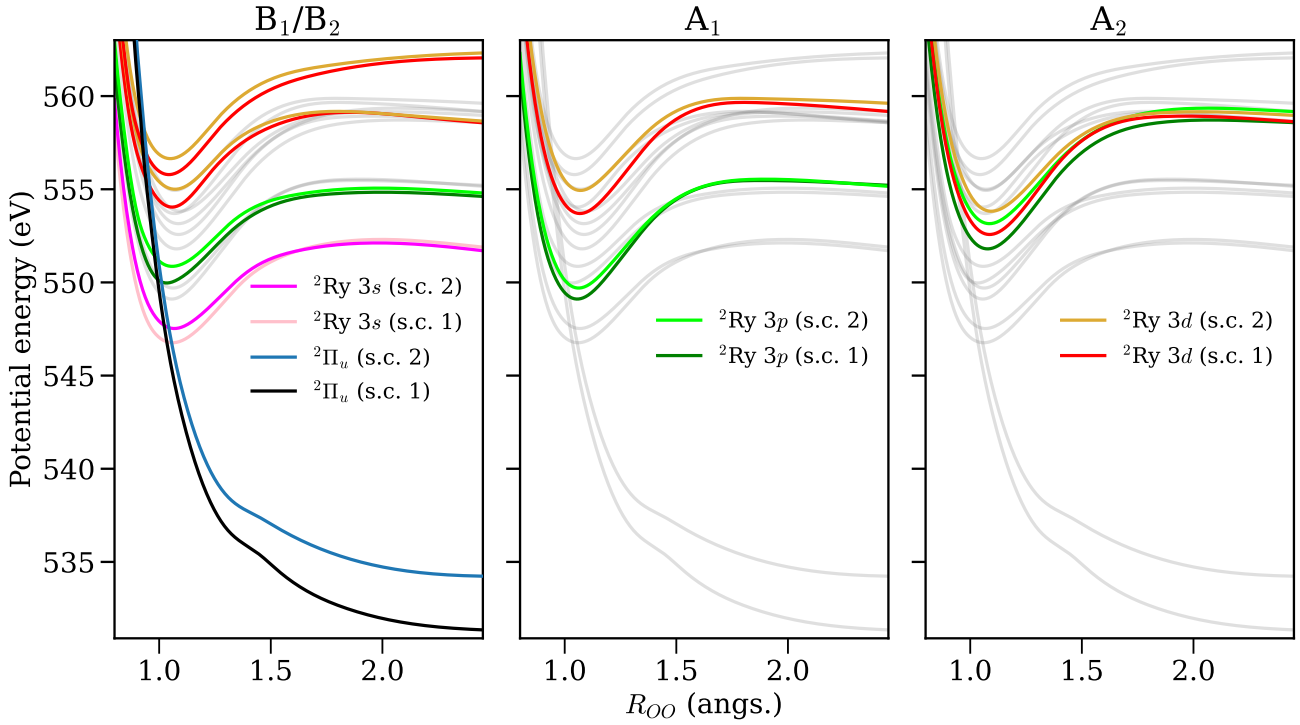

FIG. 4. Potential energy curves, in eV, for the dissociative $^2\Pi_u$ resonance ($1\sigma_g^{-1}\pi_g^1 3\sigma_u^1$) and for the first Rydberg states. The panels were divided by the symmetry of the electronic wave-function of the cation, namely B_1/B_2 (left), A_1 (middle), A_2 (right) and components. The s.c. notation in the label stands for different spin-couplings of the doublet states (see text). The color scheme follows the nature of the state, being the σ^* (blue and black lines on the B_1/B_2 panel), $1\sigma^{-1}\pi_g^1 3s^1$ (Ry) (pink and magenta - two states), $1\sigma^{-1}\pi_g^1 3p^1$ (Ry) (green and lime - six states) and $1\sigma^{-1}\pi_g^1 3d^1$ (Ry) (yellow - eight states). The energy scale is referenced at the O_2^+ ground state energy at the equilibrium geometry.

semi-internal transitions can come into play. These are defined as double excitations involving an internal excitation (occupied to partly occupied orbital) coupled to an external excitation (occupied to unoccupied orbital). Such transitions are also important in the inner parts of XPS/UPS[55] spectra and in large parts of valence Auger spectra[56, 57] as well as in related processes like the intermolecular Coulombic decay (ICD) effect [58]. It leads to the breakdown of the molecular orbital picture implying that a one-to-one mapping between orbitals and transitions is no longer possible, or expressed differently - a certain one-particle transition appears in more than one state. In the spectra of N_2^+[6], CO^+[7] and NO^+[11] many of states mixed with semi-internal transitions were predicted and observed, but with somewhat different appearance. "Normal" transitions to states having a dominating one-electron excitation with the singly occupied MO as spectator were also predicted in these spectra.

In light of these earlier findings it is interesting to inspect the energies, intensities and the dominant configurations of the transitions of the upper part of the O_2^+ XAS spectrum. These transitions appear with quite high, and irregular, relative intensity. Assignments indicate their Rydberg nature with some configuration mixing. They also appear considerably broadened as confirmed by the vibrational analysis, something that further supports their valence mixing character. In the O_2^+ case we predict that the semi-internals not only mix with Rydberg excitation, but also that groups of states appear where the semi-internals are the configurations with the largest squared coefficients, thus dominating the wave functions. The calculations predict these states are at 555-560 eV at the high energy side of the Rydberg transitions, where they probably refer to the faint structures observed in that range. They are assigned as coupled internal (mostly π to π^*) and external core to Rydberg orbital excitations. However, there is also a group of transitions predicted to be below the σ^* at 537-542 eV - this group comprises internal excitations, actually double internal excitations, where a π to π^* excitation is coupled to the core π^* excitation. To our knowledge this is the first time states of dominating internal or semi-internal character are identified in NEXAFS. Inspecting the potential curves one notes that while the two σ^* are steeply dissociative, all other states in this range are bound (Fig. 4).

V. CONCLUSION

We have presented and analyzed the XAS spectrum of O_2^+. Overall the spectrum presents some salient dif-

ferences with respect to earlier recorded XAS spectra of molecular ions. The π^* excitation comprises three states with different coupling due to the open-shell with two π_g electrons in the final state. The splitting between the states is smaller than in the corresponding resonance in isoelectronic NO, a difference which can be attributed to differences in the spatial distribution of the π orbitals. A broad spectral feature is assigned to the σ^* resonance, which is located well below the ionization limit and seemingly separated from sharper Rydberg features. It comprises two steeply dissociative states with identical electronic configuration split by their different spin coupling schemes by an amount that is determined by the exchange interaction between the two open shells. At higher energies we find complex structures which are assigned to states with mixed configurations including excitations to Rydberg states. Two groups of weak features in the high energy part of the spectrum are assigned to electron correlation states with leading internal, respectively, semi-internal configurations. The spectrum was analyzed by the RASPT2 computational method, leading to excellent agreement with the experiment which in turn made it possible to confidently assign the spectrum.

ACKNOWLEDGEMENTS

Beamtime for this project was granted at the IonTrap station of the UE52-PGM beamline at the BESSY II electron storage ring operated by the Helmholtz-Zentrum Berlin für Materialien und Energie. This project has received funding from the European Union's Horizon 2020 research and innovation programme under grant agreement No 730872 and by the German Federal Ministry of Education and Research (BMBF) through Grant No. BMBF-05K16Vf2. R.L., J.-E.R. and H. Å acknowledge funding from the Swedish Research Council, contracts 637-2014-6929, 2021-04017 and 2022-03405 respectively. The authors thank the National Academic Infrastructure for Supercomputing in Sweden (NAISS) at the National Supercomputer Centre of Linköping University partially funded by the Swedish Research Council through grant agreement no. 2022-06725.

[1] J.-P. Mosnier, E. T. Kennedy, P. van Kampen, D. Cubaynes, S. Guilbaud, N. Sisourat, A. Puglisi, S. Carniato, and J.-M. Bizau, Inner-shell photoexcitations as probes of the molecular ions ch^+, oh^+, and sih^+: Measurements and theory, Phys. Rev. A **93**, 061401 (2016).

[2] S. Klumpp, A. A. Guda, K. Schubert, K. Mertens, J. Hellhund, A. Müller, S. Schippers, S. Bari, and M. Martins, Photoabsorption of the molecular IH cation at the iodine 3 d absorption edge, Physical Review A **97**, 033401 (2018).

[3] S. Bari, L. Inhester, K. Schubert, K. Mertens, J. O. Schunck, S. Dörner, S. Deinert, L. Schwob, S. Schippers, A. Müller, *et al.*, Inner-shell x-ray absorption spectra of the cationic series NH_y^+(y= 0–3), Physical Chemistry Chemical Physics **21**, 16505 (2019).

[4] K. Schubert, A. A. Guda, K. Mertens, J. O. Schunck, S. Schippers, A. Müller, S. Bari, S. Klumpp, and M. Martins, Absorption spectra at the iodine 3d ionisation threshold following the chxi+ (x = 0–3) cation sequence, Phys. Chem. Chem. Phys. **21**, 25415 (2019).

[5] E. T. Kennedy, J. P. Mosnier, P. V. Kampen, J. M. Bizau, D. Cubaynes, S. Guilbaud, S. Carniato, A. Puglisi, and N. Sisourat, Vibrational effects in the photo-ion yield spectrum of the sih2+ molecular ion following 2p inner-shell excitation, Journal of Physics: Conference Series **1289**, 012003 (2019).

[6] R. Lindblad, L. Kjellsson, R. C. Couto, M. Timm, C. Bülow, V. Zamudio-Bayer, M. Lundberg, B. von Issendorff, J. T. Lau, S. L. Sorensen, V. Carravetta, H. Ågren, and J.-E. Rubensson, X-ray absorption spectrum of the N_2^+ molecular ion, Phys. Rev. Lett. **124**, 203001 (2020).

[7] R. C. Couto, L. Kjellsson, H. Ågren, V. Carravetta, S. L. Sorensen, M. Kubin, C. Bülow, M. Timm, V. Zamudio-Bayer, B. Von Issendorff, J. T. Lau, J. Söderström, J.-E. Rubensson, and R. Lindblad, The carbon and oxygen k-edge nexafs spectra of CO^+, Physical Chemistry Chemical Physics **22**, 16215 (2020).

[8] S. Carniato, J.-M. Bizau, D. Cubaynes, E. T. Kennedy, S. Guilbaud, E. Sokell, B. McLaughlin, and J.-P. Mosnier, Vibrationally and spin-orbit-resolved inner-shell x-ray absorption spectroscopy of the nh+ molecular ion: Measurements and ab initio calculations, Atoms **8**, 10.3390/atoms8040067 (2020).

[9] M. Martins, S. Reinwardt, J. O. Schunck, J. Schwarz, K. Baev, A. Müller, T. Buhr, A. Perry-Sassmannshausen, S. Klumpp, and S. Schippers, Disentangling the photodissociation dynamics of the hf+ molecular radical via kinetic-energy-release-resolved f 1s core excitation and ionization, *The Journal of Physical Chemistry Letters*, The Journal of Physical Chemistry Letters **12**, 1390 (2021).

[10] R. C. Couto, W. Hua, R. Lindblad, L. Kjellsson, S. L. Sorensen, M. Kubin, C. Bülow, M. Timm, V. Zamudio-Bayer, B. von Issendorff, J. Söderström, J. T. Lau, J.-E. Rubensson, H. Ågren, and V. Carravetta, Breaking inversion symmetry by protonation: experimental and theoretical nexafs study of the diazynium ion, n2h+, Phys. Chem. Chem. Phys. **23**, 17166 (2021).

[11] R. Lindblad, L. Kjellsson, E. De Santis, V. Zamudio-Bayer, B. von Issendorff, S. L. Sorensen, J. T. Lau, W. Hua, V. Carravetta, J.-E. Rubensson, H. Ågren, and R. C. Couto, Experimental and theoretical near-edge x-ray-absorption fine-structure studies of no^+, Phys. Rev. A **106**, 042814 (2022).

[12] J. Schwarz, F. Kielgast, I. Baev, S. Reinwardt, F. Trinter, S. Klumpp, A. Perry-Sassmannshausen, T. Buhr, S. Schippers, A. Müller, S. Bari, V. Mondes, R. Flesch, E. Rühl, and M. Martins, X-ray absorption spectroscopy

of h3o+, Phys. Chem. Chem. Phys. **24**, 23119 (2022).
[13] S. Schippers, P.-M. Hillenbrand, A. Perry-Sassmannshausen, T. Buhr, S. Fuchs, S. Reinwardt, F. Trinter, A. Müller, and M. Martins, Vibrationally resolved inner-shell photoexcitation of the molecular anion c2, ChemPhysChem **24**, e202300061 (2023).
[14] V. Carravetta, R. C. Couto, and H. Ågren, X-ray absorption of molecular cations—a new challenge for electronic structure theory, Journal of Physics: Condensed Matter **34**, 363002 (2022).
[15] L. Young, K. Ueda, M. Gühr, P. H. Bucksbaum, M. Simon, S. Mukamel, N. Rohringer, K. C. Prince, C. Masciovecchio, M. Meyer, A. Rudenko, D. Rolles, C. Bostedt, M. Fuchs, D. A. Reis, R. Santra, H. Kapteyn, M. Murnane, H. Ibrahim, F. Légaré, M. Vrakking, M. Isinger, D. Kroon, M. Gisselbrecht, A. L'Huillier, H. J. Wörner, and S. R. Leone, Roadmap of ultrafast x-ray atomic and molecular physics, Journal of physics. B, Atomic, molecular, and optical physics **51**, 32003 (2018).
[16] M. Chergui, M. Beye, S. Mukamel, C. Svetina, and C. Masciovecchio, Progress and prospects in nonlinear extreme-ultraviolet and x-ray optics and spectroscopy, Nature Reviews Physics **5**, 578 (2023).
[17] C. H. Yuen and C. D. Lin, Quantifying robustness of attosecond transient absorption spectroscopy for vibronic coherence in charge migration (2023), arXiv:2307.13819 [physics.atom-ph].
[18] V. Kimberg, A. Sanchez-Gonzalez, L. Mercadier, C. Weninger, A. Lutman, D. Ratner, R. Coffee, M. Bucher, M. Mucke, M. Agåker, *et al.*, Stimulated x-ray raman scattering–a critical assessment of the building block of nonlinear x-ray spectroscopy, Faraday Discuss. **194**, 305 (2016).
[19] N. L. Aleksandrov, E. M. Bazelyan, A. A. Ponomarev, and A. Y. Starikovsky, Kinetics of charged species in non-equilibrium plasma in water vapor- and hydrocarbon-containing gaseous mixtures, Journal of Physics D: Applied Physics **55**, 383002 (2022).
[20] N. S. Shuman, D. E. Hunton, and A. A. Viggiano, Ambient and modified atmospheric ion chemistry: From top to bottom, *Chemical Reviews*, Chemical Reviews **115**, 4542 (2015).
[21] T. P. Snow and V. M. Bierbaum, Ion chemistry in the interstellar medium, Annual Review of Analytical Chemistry **1**, 229 (2008), pMID: 20636080, https://doi.org/10.1146/annurev.anchem.1.031207.112907.
[22] K. Hirsch, J. T. Lau, P. Klar, A. Langenberg, J. Probst, J. Rittmann, M. Vogel, V. Zamudio-Bayer, T. Möller, and B. von Issendorff, X-ray spectroscopy on size-selected clusters in an ion trap: from the molecular limit to bulk properties, J. Phys. B **42**, 154029 (2009).
[23] R. Ovsyannikov and T. Lau, The variable polarization undulator beamline UE52 PGM nanocluster trap at bessy ii, Journal of large-scale research facilities JLSRF **3**, 105 (2017).
[24] H. Ågren, A. Flores-Riveros, and H. Jensen, An Efficient Method for Calculating Molecular Radiative Intensities in the VUV and Soft X-ray Wavelength Regions, Phys. Scr. **40**, 745 (1989).
[25] H. J. A. Jensen, P. Jørgensen, and H. Ågren, Efficient optimization of large scale MCSCF wave functions with a restricted step algorithm, J. Chem. Phys. **87**, 451 (1987).
[26] P. Å. Malmqvist, A. Rendell, and B. O. Roos, The restricted active space self-consistent-field method, implemented with a split graph unitary group approach, J. Phys. Chem. **94**, 5477 (1990).
[27] G. Li Manni, I. Fdez. Galván, A. Alavi, F. Aleotti, F. Aquilante, J. Autschbach, D. Avagliano, A. Baiardi, J. J. Bao, S. Battaglia, L. Birnoschi, A. Blanco-González, S. I. Bokarev, R. Broer, R. Cacciari, P. B. Calio, R. K. Carlson, R. Carvalho Couto, L. Cerdán, L. F. Chibotaru, N. F. Chilton, J. R. Church, I. Conti, S. Coriani, J. Cuéllar-Zuquin, R. E. Daoud, N. Dattani, P. Decleva, C. de Graaf, M. G. Delcey, L. De Vico, W. Dobrautz, S. S. Dong, R. Feng, N. Ferré, M. Filatov(Gulak), L. Gagliardi, M. Garavelli, L. González, Y. Guan, M. Guo, M. R. Hennefarth, M. R. Hermes, C. E. Hoyer, M. Huix-Rotllant, V. K. Jaiswal, A. Kaiser, D. S. Kaliakin, M. Khamesian, D. S. King, V. Kochetov, M. Krośnicki, A. A. Kumaar, E. D. Larsson, S. Lehtola, M.-B. Lepetit, H. Lischka, P. López Ríos, M. Lundberg, D. Ma, S. Mai, P. Marquetand, I. C. D. Merritt, F. Montorsi, M. Mörchen, A. Nenov, V. H. A. Nguyen, Y. Nishimoto, M. S. Oakley, M. Olivucci, M. Oppel, D. Padula, R. Pandharkar, Q. M. Phung, F. Plasser, G. Raggi, E. Rebolini, M. Reiher, I. Rivalta, D. Roca-Sanjuán, T. Romig, A. A. Safari, A. Sánchez-Mansilla, A. M. Sand, I. Schapiro, T. R. Scott, J. Segarra-Martí, F. Segatta, D.-C. Sergentu, P. Sharma, R. Shepard, Y. Shu, J. K. Staab, T. P. Straatsma, L. K. Sørensen, B. N. C. Tenorio, D. G. Truhlar, L. Ungur, M. Vacher, V. Veryazov, T. A. Voß, O. Weser, D. Wu, X. Yang, D. Yarkony, C. Zhou, J. P. Zobel, and R. Lindh, The openmolcas web: A community-driven approach to advancing computational chemistry, Journal of Chemical Theory and Computation DOI: 10.1021/acs.jctc.3c00182.
[28] R. Püttner, I. Dominguez, T. J. Morgan, C. Cisneros, R. F. Fink, E. Rotenberg, T. Warwick, M. Domke, G. Kaindl, and A. S. Schlachter, Vibrationally resolved O 1*s* core-excitation spectra of CO and NO, Phys. Rev. A **59**, 3415 (1999).
[29] S. Sorensen, K. Børve, R. Feifel, A. De Fanis, and K. Ueda, The O 1s photoelectron spectrum of molecular oxygen revisited, Journal of Physics B: Atomic, Molecular and Optical Physics **41**, 095101 (2008), publisher: IOP Publishing.
[30] M. R. Weiss, R. Follath, K. J. S. Sawhney, and T. Zeschke, Absolute energy calibration for plane grating monochromators, Nuclear Instruments and Methods in Physics Research Section A: Accelerators, Spectrometers, Detectors and Associated Equipment **467-468**, 482 (2001).
[31] P. Baltzer, B. Wannberg, L. Karlsson, M. Carlsson Göthe, and M. Larsson, High-resolution inner-valence uv photoelectron spectra of the O_2 molecule and configuration-interaction calculations of $^2\Pi_u$ states between 20 and 26 eV, Phys. Rev. A **45**, 4374 (1992).
[32] E. Andersson, M. Stenrup, J. H. D. Eland, L. Hedin, M. Berglund, L. Karlsson, A. Larson, H. Ågren, J.-E. Rubensson, and R. Feifel, Single-photon core-valence double ionization of molecular oxygen, Phys. Rev. A **78**, 023409 (2008).
[33] V. Carravetta, R. C. Couto, and H. Ågren, X-ray absorption of molecular cations—a new challenge for electronic structure theory, Journal of Physics: Condensed Matter **34**, 363002 (2022).
[34] P. Å. Malmqvist, K. Pierloot, A. R. M. Shahi, C. J. Cramer, and L. Gagliardi, The restricted active space fol-

lowed by second-order perturbation theory method: Theory and application to the study of Cu O 2 and Cu 2 O 2 systems, J. Chem. Phys. **128**, 204109 (2008).

[35] L. S. Cederbaum, W. Domcke, and J. Schirmer, Many-body theory of core holes, Phys. Rev. A **22**, 206 (1980).

[36] M. G. Delcey, L. K. Sørensen, M. Vacher, R. C. Couto, and M. Lundberg, Efficient calculations of a large number of highly excited states for multiconfigurational wavefunctions, J. Comp. Chem. **40**, 1789 (2019).

[37] K. Kaufmann, W. Baumeister, and M. Jungen, Universal gaussian basis sets for an optimum representation of rydberg and continuum wavefunctions, Journal of Physics B: Atomic, Molecular and Optical Physics **22**, 2223 (1989).

[38] M. Douglas and N. M. Kroll, Quantum electrodynamical corrections to the fine structure of helium, Ann. Phys. **82**, 89 (1974).

[39] B. A. Hess, Relativistic electronic-structure calculations employing a two-component no-pair formalism with external-field projection operators, Phys. Rev. A **33**, 3742 (1986).

[40] P.-Å. Malmqvist and B. O. Roos, The CASSCF state interaction method, Chem. Phys. Lett. **155**, 189 (1989).

[41] P. Å. Malmqvist, B. O. Roos, and B. Schimmelpfennig, The restricted active space (RAS) state interaction approach with spin–orbit coupling, Chem. Phys. Lett. **357**, 230 (2002).

[42] J. Pipek and P. G. Mezey, A fast intrinsic localization procedure applicable for abinitio and semiempirical linear combination of atomic orbital wave functions, J. Chem. Phys. **90**, 4916 (1989).

[43] N. Forsberg and P.-Å. Malmqvist, Multiconfiguration perturbation theory with imaginary level shift, Chem. Phys. Lett. **274**, 196 (1997).

[44] G. Ghigo, B. O. Roos, and P.-Å. Malmqvist, A modified definition of the zeroth-order hamiltonian in multiconfigurational perturbation theory (caspt2), Chem. Phys. Lett. **396**, 142 (2004).

[45] F. Gel'mukhanov and H. Ågren, Resonant X-ray Raman Scattering, Phys. Rep. **312**, 87 (1999).

[46] M. Coreno, M. de Simone, K. Prince, R. Richter, M. Vondráček, L. Avaldi, and R. Camilloni, Vibrationally resolved oxygen k→ spectra of o2 and co, Chemical Physics Letters **306**, 269 (1999).

[47] F. Frati, M. O. J. Y. Hunault, and F. M. F. de Groot, Oxygen k-edge x-ray absorption spectra, Chemical Reviews **120**, 4056 (2020), pMID: 32275144, https://doi.org/10.1021/acs.chemrev.9b00439.

[48] N. Kosugi, J. Adachi, E. Shigemasa, and A. Yagishita, High-resolution and symmetry-resolved N and O K-edge absorption spectra of NO, The Journal of Chemical Physics **97**, 8842 (1992).

[49] J. Müller and H.Ågren, in *Proceedings of NATO ASI Conference on Molecular Ions*, edited by J. Berkowitz (Plenum Publ. Corp., 1980).

[50] K. Huber and G. Herzberg, *Molecular structure and molecular spectra, Vol. 4. Constants of diatomic molecules* (Van Nostrand Reinhold, New York, 1979).

[51] A. Yagishita, E. Shigemasa, and N. Kosugi, Observation of rydberg-valence mixing in high-resolution symmetry-resolved oxygen k-edge spectra of o2, Physical Review Letters **72**, 3961 (1994), cited by: 79.

[52] R. Püttner and K. Ueda, The angularly resolved O 1s ion-yield spectrum of O_2 revisited, The Journal of Chemical Physics **145**, 224302 (2016).

[53] A. Lindblad, V. Kimberg, J. Söderström, C. Nicolas, O. Travnikova, N. Kosugi, F. Gel'mukhanov, and C. Miron, Vibrational scattering anisotropy in o2—dynamics beyond the born–oppenheimer approximation, New Journal of Physics **14**, 113018 (2012).

[54] H. Ågren and R. Arneberg, Physica Scripta **119**, 297 (1984).

[55] L. Cederbaum, A simple explanation of the breakdown of koopmans' theorem for f2 and n2, Chemical Physics Letters **25**, 562 (1974).

[56] H. Ågren and H. Siegbahn, Semi-internal correlation in the auger electron spectrum of h2o, Chemical Physics Letters **69**, 424 (1980).

[57] H. Ågren, On the interpretation of molecular valence Auger spectra, The Journal of Chemical Physics **75**, 1267 (1981).

[58] L. S. Cederbaum, J. Zobeley, and F. Tarantelli, Giant intermolecular decay and fragmentation of clusters, Phys. Rev. Lett. **79**, 4778 (1997).